Composites Science and Technology 68 (2008) 3337–3343

Contents lists available at ScienceDirect

Composites Science and Technology

journal homepage: www.elsevier.com/locate/compscitech

A self-healing smart syntactic foam under multiple impacts

Guoqiang Li [a,b,*], Manu John [a]

[a] Department of Mechanical Engineering, Louisiana State University, Baton Rouge, LA 70803, USA
[b] Department of Mechanical Engineering, Southern University, Baton Rouge, LA 70813, USA

ARTICLE INFO

Article history:
Received 1 June 2008
Received in revised form 21 August 2008
Accepted 3 September 2008
Available online 15 September 2008

Keywords:
C: Sandwich
A: Smart materials
A: Nanocomposites
B: Impact behavior
Syntactic foam

ABSTRACT

In this study, a shape memory polymer (SMP) based syntactic foam and the foam cored sandwich structures were developed for the purpose of repeatedly self-healing impact damage. The foam was made of shape memory polystyrene, glass microballoon, and multi-walled carbon nanotube. The foam cored composite sandwich plates were prepared per the vacuum assisted resin infusion molding (VARIM) technology. A stress-controlled programming was coupled with the curing process of the sandwich plates for shape fixity. The foam was characterized per TEM, DSC, and flat-wise compression test. The sandwich panels were subjected to seven rounds of impact-healing cycles. C-scan and SEM were used to characterize the impact damage and healing efficiency. The impact response was characterized per the load and energy traces. The impact damaged and healed sandwich specimens were then tested using the compression after impact (CAI) tests to evaluate their residual load carrying capacity. The test results show that the impact damage can be healed under multiple impacts and the impact tolerance and residual strength can be recovered. It is also found that coupling the programming with sandwich curing is an effective way of making the foam smart.

1. Introduction

Syntactic foam, a class of structural materials obtained by dispersing microballoons into a polymeric or metallic matrix, has enjoyed continuously increasing growth in composite sandwich structures in recent years. The history of polymeric matrix syntactic foams dated back to the 1950s to 1960s. They were first developed as buoyancy materials for submarines, thermo insulation materials for buildings, trains, and aircraft, cushion materials for packing, etc. [1–3]. Since 1980s, in particular 1990s, syntactic foams have gained new momentum partly due to the increased application of foam cored composite sandwich structures in various civilian and military structures. A comprehensive and detailed survey on syntactic foams and related literature was provided by Shutov [4,5]. Recent development in polymeric syntactic foams include static and dynamic modeling of the constitutive behavior of syntactic foams by using analogy to geomaterials [6] or using damage mechanics [7]; modeling of the effective elastic properties based on micromechanics, homogenization, and equivalent medium theorem [8,9]; toughened syntactic foam by coating microballoons with rubber latex or adding crumb rubber particles into the polymer matrix [10–12]; and functionally graded syntactic foam by changing the volume fraction of the microballoons or changing the density of the microballoons as the spatial location changes [13,14]. It is well known that the current polymeric syntactic foam cored sandwich usually has a very low post-impact residual bearing capacity due to its micro/macroscopic damage and lack of capacity for self-healing the damage [10–12,15–18].

Self-healing of structural damage has been a tremendous interest in the scientific community recently [19,20]. The first self-healing material utilized microcapsules which enclosed a monomeric fluid and catalysts were dispersed throughout the matrix material. When a propagating crack encounters one of the dispersed capsules, the capsule bursts and the encased fluid flows into the cracked region. Catalyst in the vicinity initiates an *in-situ* polymerization reaction and thus patches the crack. Obviously, this self-healing plan is a one time deal [21]. It cannot be used more than once. Some modified versions of this idea such as a self-healing system that simulates the human circulatory system [22] or triggers the self-healing process by impact [23], which may heal damage more than one time, suffer from new challenges such as the microcapsules are driven to burst and discharge their entire payload at a damaged region, thereby delivering a high concentration of healing agents to a small area.

The discovery of shape memory effect by Chang and Read in 1932 [24] is one of the revolutionary steps in the field of active materials research. Among the various shape memory materials such as shape memory alloy (SMA, for instance Ni–Ti alloy), shape memory ceramic, and shape memory polymer (SMP), SMPs have

* Corresponding author. Address: Department of Mechanical Engineering, Louisiana State University, Baton Rouge, LA 70803, USA. Tel.: +1 225 578 5302; fax: +1 225 578 5924.
E-mail address: guoli@me.lsu.edu (G. Li).

0266-3538/$ - see front matter © 2008 Elsevier Ltd. All rights reserved.
doi:10.1016/j.compscitech.2008.09.009

drawn increasing attention because of their scientific and technological significance [24,25]. SMP was first developed by CDF Chimie Company (France) in 1984 under the trade name of Polynorbornene [24]. It was found that SMP offers deformation to a much higher degree and a wider scope of varying mechanical properties compared to SMAs or ceramics. The driving force for shape recovery is the conformational entropy of the molecular segments in terms of micro-Brownian thermal motion. Thermodynamically, the molecular segments experience a change from a temporary and ordered configuration to its random and coiled configuration during the shape recovery process. Since this process is accompanied by an increase in entropy, it is an autonomous process. It is the recovery in strain and in stress that makes SMP a viable choice as sensors and actuators. In order to make the polymer smart, it usually experiences a typical four-step thermomechanical cycle called programming [24–26]. For a strain-controlled programming, it starts at a temperature above the glass transition temperature (T_g) of the SMP. It involves a high-strain deformation in the rubbery state, which is called pre-deformation or pre-strain. Step 2 is a strain storage process by maintaining the pre-strain constant while cooling down to below T_g. The third Step is a low temperature unloading process, which is defined as the removal of the stress in the glassy state. In Step 4, which involves reheating to its starting temperature (above T_g) without applying any constraint, sometimes called free strain recovery or unconstrained recovery, brings the pre-strain back to zero (if the recovery rate is 100%).

The idea in this study is to utilize the shape memory functionality of SMP to serve the purpose of self-healing damage. It is envisioned that SMPs will outperform the current self-healing schemes because it is driven by conformational entropy and thus the self-healing is autonomous; the self-healing is controllable by controlling the programming; and the self-healing can be repeated. In this study, we developed a SMP based syntactic foam and prepared the foam cored sandwich. The programming was conducted by association with the sandwich curing process. The foam was characterized by DSC, TEM, and flat-wise uniaxial compression test. Low velocity impact tests up to seven impact-healing cycles were conducted on the foam cored sandwich structures at room temperature, and the impact damage was evaluated by SEM and C-Scan. Compression after impact (CAI) test was also conducted to evaluate the residual load carrying capacity of the foam cored sandwich structures.

2. Specimens preparation and experimentation

2.1. Raw materials

The syntactic foam was fabricated by dispersing glass microballoons and multi-walled carbon nanotubes into a shape memory polymer matrix. The shape memory polymer (polystyrene, CRG industries) has a T_g of 62 °C, tensile strength of 23 MPa and modulus of elasticity of 1.24 GPa at room temperature. The foam was fabricated by dispersing 40% by volume of glass microballoons (Potters Industries Q-cel 6014: bulk density of 0.08 g/cm^3, effective density of 0.14 g/cm^3, particle diameter range of 5–200 μm, average diameter of 85 μm, and crushing strength of 1.72 MPa), and 0.15% by volume of multi-walled carbon nanotubes (Cheap Tubes Inc.: density of 2.1 g/cm^3, diameter of 20–30 nm, and length of 20–30 μm) into the polymer matrix. Carbon nanotubes were used for a couple of reasons. One is that carbon nanotubes can enhance the strength, stiffness, and recovery rate of the SMP matrix, which is critical when the temperature is higher than T_g; the other is that carbon nanotubes have a potential to serve as a medium for heating and triggering phase change if its content is higher than the percolation threshold, such as by infrared light or electricity [27,28].

2.2. Syntactic foam and the foam cored sandwich fabrication

A two-step procedure was used to prepare the syntactic foam. First, the carbon nanotubes were added to the polymer matrix. The mixture was mixed with the assistance of an ultrasound mixer for 30 min at a frequency of 20 kHz (Sonics Vibracell VC 750 W) and a three-roll mill for one pass (NETZSCH type 50). It was found that this combination was adequate to uniformly distribute the carbon nanotubes in the polymer matrix; see a TEM picture in Fig. 1. Second, microballoons and hardener were added to the carbon nanotube/polymer mixture and mixed with a spatula for 15 min. It was then poured into an aluminum mold for curing. The process started with 24 h of room temperature curing, followed by post-curing at 75 °C for 24 h, 90 °C for 3 h and 100 °C for 3 h in an oven. This curing cycle was chosen by a *trial and error* process because the curing cycle for the pure polymer recommended by the manufacturer cannot cure the foam.

After curing, the foam cored sandwich panels with a dimension of 152.4 × 101.6 × 12.7 mm were prepared for impact and self-healing tests. This particular dimension was selected in order to conduct compression after impact test per the anti-buckling test fixture. The sandwich plates were fabricated using the Vacuum Assisted Resin Infusion Molding (VARIM) system (Airtech). In order to keep chemical compatibility, the polymer used in the skin was the same shape memory polymer as the foam core. The cured thickness of the skin was 0.736 mm. After curing the sandwich at room temperature for 24 h, it was post-cured by coupling with programming or shape fixity of the foam core.

2.3. Programming

In this study, the shape fixity or programming of the smart foam core was coupled with the post-curing of the sandwich panels. The programming was similar to the regular, four-step strain-controlled programming. However, we used stress-controlled programming with a constant compressive stress of 0.05 MPa in this study. The programming started by heating the sandwich panel to 75 °C. After that, the pressure of 0.05 MPa was applied by the vacuum system. This temperature and pressure was maintained for 24 h. After that the temperature was raised to 90 °C and maintained for 3 h. The sandwich was then heated up to 100 °C and the temperature was maintained for another 3 h (Step 1). Then the sandwich panel was cooled down to room temperature in about 6 h while maintaining the stress level (Step 2). After about 0.5 h at room temperature, the pressure was removed (Step 3). This completed the three-step of shape fixity process and the sandwich panels were ready for impact testing.

In order to examine the shape recovery capacity, the fourth Step was also conducted on a control sandwich panel. The

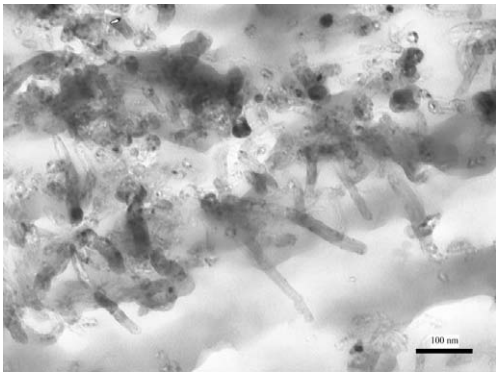

Fig. 1. TEM picture of the carbon nanotubes in the SMP matrix.

sandwich panel was heated up again to 100 °C to determine the shape recovery without applying any stress (free or unconstrained shape recovery). In order to quantitatively obtain the four-step thermal–mechanical programming cycle, strain gages were installed along the edges of the control sandwich panel in the thickness direction in order to determine the through-thickness strain. A Yokogawa DC100 device was used to monitor the changes of strain with time and temperature. The temperature was monitored with the help of thermocouples connected to the same device.

2.4. Uniaxial compression test of the foam

In order to evaluate the mechanical properties of the prepared foam, uniaxial compression test was conducted. The foam specimens were 25.0 mm long, 25.0 mm wide, and 12.5 mm thick blocks, which were tested flat-wise per ASTM C 365 using an MTS 810 machine. The test was strain controlled and the loading rate was 1.3 mm/min. The test was conducted at room temperature. Three effective specimens were tested. The stress–strain curve was obtained and the yield strength, ultimate strength, and modulus of elasticity were determined. Yield strength suggests the end of elastic region and start of elastic–plastic region. The ultimate strength suggests the maximum load carrying capacity of the specimen. A similar study for the pure SMP and the pure SMP with 0.15% by volume of carbon nanotubes was also conducted to evaluate the effect of the carbon nanotubes on the shape recovery rate of the SMP. Three effective specimens were tested for each type of materials. The shape fixity rate for both types of specimens was 60%. After that, the specimens were brought to an oven at 100 °C for 3 h for free shape recovery.

2.5. Differential scanning calorimetry (DSC) test

In order to determine the effect of the elastic constituents (glass microballoon and multi-walled carbon nanotube) on the glass transition temperature of the SMP matrix, a DSC test using a TA instruments Q-series thermal analysis DSC was conducted on the foam. Specimens weighing a few milligrams were used and the test was conducted from 35 °C to 100 °C at a ramping rate of 5 °C/min. Three effective specimens were tested to obtain an average glass transition temperature value.

2.6. Low velocity impact test

Low velocity impact tests were performed on each sandwich panel at the same impact location (center of the panel) repeatedly using an Instron Dynatup 8250 HV drop tower machine at a velocity of 3 m/s and a hammer weight of 6.64 kg per ASTM D 2444. The impact tests were conducted at room temperature. After each impact, the specimen was brought to an oven for unconstrained shape recovery (healing) at a temperature of 100 °C for 3 h. This impact-healing process was repeated for seven cycles. For each impact at least five effective specimens were tested and the load and energy traces were obtained. The maximum impact force, maximum deflection, and impact duration were directly obtained from the load and energy traces. The initiation energy and propagation energy were calculated based on the traces. Impact energy corresponding to the maximum impact force is defined as initiation energy. Propagation energy is defined as the difference between the maximum impact energy and the initiation energy. These definitions have been used previously [10–12]. It has been suggested that the initiation energy is basically a measurement of the capacity for the target to transfer energy elastically and a higher initiation energy usually means a higher load carrying capacity; on the other hand, the propagation energy represents the energy absorbed by the target for creating and propagating gross damage.

2.7. Ultrasonic and SEM inspection

Ultrasonic inspection was performed on all specimens both after impact and after healing for each impact-healing cycle using a 1 MHz transducer. An UltraPac inspection machine from Physical Acoustics Laboratory was used in conjunction with UltraWin software to acquire the C-scan images and identify damages. Scanning electron microscope (SEM) observation of micro-length scale damage was conducted using a JEOL JSM-840A scanning electron microscope.

2.8. Compression after impact test

The testing was conducted using a MTS 810 machine and the fixture used was a "Boeing Compression after Impact Compression Test Fixture" per BSS7260 standard. The size of the specimen was 152.4 mm long, 101.6 mm wide, and 12.7 mm thick. At least five effective specimens were tested for each parameter considered. A strain controlled testing mode was used during the testing and the loading rate was 5.0 mm/min.

3. Results and discussion

3.1. Thermal–mechanical cycle

The programming of the smart foam cored sandwich is shown in Fig. 2. The four-steps associated with the shape fixity and shape recovery are highlighted in the figure. Fixity and recovery rates are two parameters used to determine the characteristics of SMPs. In the literature, the fixity and recovery rates are determined in terms of strain [25]

$$R_f(N) = \frac{\varepsilon_u(N)}{\varepsilon_m}, \text{ and } R_r(N) = \frac{\varepsilon_m - \varepsilon_p(N)}{\varepsilon_m - \varepsilon_p(N-1)} \quad (1)$$

where N is the number of thermomechanical cycles ($N = 1$ in Fig. 2); R_f is the shape fixity rate; ε_m is the pre-deformation strain (strain at the end of Step 2); ε_u is the temporary strain fixed (strain at the end of Step 3); R_r is the shape recovery rate; and ε_p is the permanent strain (strain at the end of Step 4).

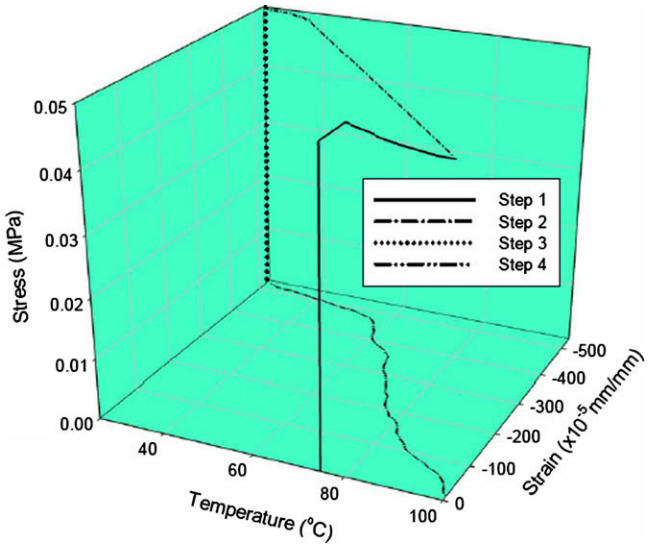

Fig. 2. Four-step thermomechanical programming cycle.

From Fig. 2, it is found that the shape fixity rate $R_f = (529 \times 10^{-5}\ \text{mm/mm})/(534 \times 10^{-5}\ \text{mm/mm}) = 99\%$. The shape recovery rate $R_r = (534 \times 10^{-5}\ \text{mm/mm} - 13 \times 10^{-5}\ \text{mm/mm})/(534 \times 10^{-5}\ \text{mm/mm} - 0 \times 10^{-5}\ \text{mm/mm}) = 97.6\%$. From the above calculation, it is clear that the shape fixity rate is very high and the shape recovery rate is close to 100%, suggesting good shape memory functionality of the smart foam. Also, a turning point is found in the shape recovery step (Step 4) around the glass transition temperature of the SMP (62° C).

3.2. Flat-wise compression test

A typical compressive stress-strain behavior of the foam is shown in Fig. 3. It is clear that the stress–strain curve can be characterized by three distinct regions. The initial region is a linear elastic region. This is followed by a plateau region which corresponds to the rubbery deformation of the foam matrix; the last region sees the compaction and consolidation of the foam material, which may include the crushing and densification of the microballoons. Compared with regular syntactic foam, it is obvious that the deformation in the rubbery region is much higher. This suggests that the smart foam would be able to absorb more impact energy without disintegration.

The test results also show that the 100° C, 3-h free shape recovery rate for the neat SMP is 96.7%, while it is 99.3% for the SMP reinforced with 0.15% by volume of carbon nanotubes. Obviously, this confirms that the incorporation of carbon nanotubes enhances the shape recovery rate of SMP as expected.

3.3. Differential scanning calorimetry (DSC) test

The DSC test results of the foam are shown in Fig. 4. The three curves are parallel tests of three specimens. From Fig. 4, there is a change of slope at about 62° C, the glass transition temperature of the polymer matrix. This suggests that the glass transition temperature of the foam is around 62° C. However, it is noted that the peak has been significantly flattened, possibly due to the elastic constituents (carbon nanotubes and glass microballoons) contained in the foam, which have constant heat flow. This type of flattened peak was also observed by others in carbon nanotube reinforced shape memory polymer [29].

3.4. Low velocity impact test

Typical load and energy traces are shown in Fig. 5. The maximum impact force, maximum deflection, impact duration, initiation energy, and propagation energy after each impact are summarized in Fig. 6. From Fig. 6, the impact response is statistically the same for each round of impact. This suggests that the damage induced by each impact has been effectively healed by the shape recovery process. The impact tolerance has been effectively recovered by self-healing. Actually, it seems that the impact tolerance after the 7th round of impact is slightly better than that after the 1st round of impact, as indicated by a slightly higher initiation energy and a slightly lower propagation energy. This 'abnormal' behavior suggests that repeated impact and healing cycles may have adjusted the microstructure of the foam, making it more beneficial for impact tolerance. Another possible reason is the post-curing effect caused by the healing process, which was conducted for 3 h at 100° C for each healing cycle. This will be further discussed in Section 3.6.

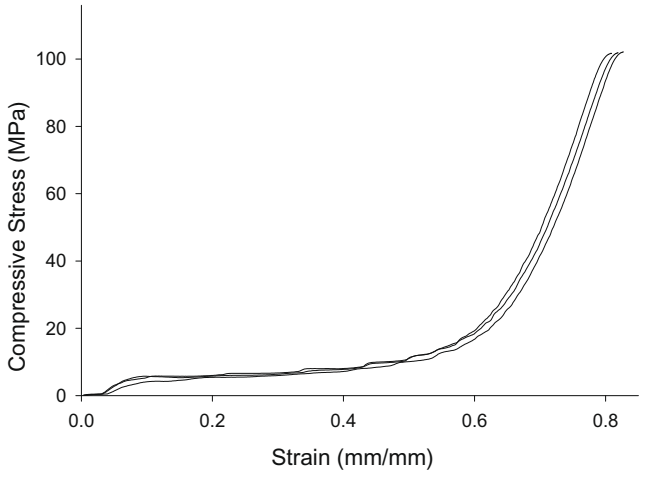

Fig. 3. Typical compressive stress–strain curves for the foam material.

3.5. C-scan and SEM observation

The impact damage can be visualized by C-scan and the damage at micro-length scale can be observed by SEM. Fig. 7 shows the C-scan results of one sandwich panel before impact, after 1st impact, after 1st healing, until after 7th impact and 7th healing. In these pulse-echo C-scan images, red color represents an excess of 80% of the signal returning to the receiver, whereas blue color indicates that 50–80% of the signal is being received. White color represents a complete attenuation of the ultrasound signal or 0% of signal received. Therefore, the white spot at the center of the specimen indicates a certain type of damage. Two observations can be made: (1) the damage after each impact has been effectively healed, as evidenced by the removal of the white spot; (2) the microstructure has been changed after each impact-healing cycle as indicated by the change of the color distribution. These observations are supported by the impact responses, which show that the healing has helped the sandwich panel not only recover, but also slightly enhance its impact tolerance.

Fig. 8 shows a comparison of a microcrack in the foam core immediately after impact and immediately after healing. It is clear that the microcrack length has been reduced and the microcrack opening has been narrowed after healing. It is noted that during healing the sample, the shape recovery is stress-free, i.e., unconfined free shape recovery. In the sandwich panel, the foam core directly under impact is partially confined by the skin and by the surrounding materials. Therefore, the confinement may produce a certain stress which may help in pushing the microcrack from two sides and thus may help close the crack. In another word, the microcrack in actual sandwich panels may have a better healing effect than that seen in Fig. 8.

3.6. Compression after impact (CAI) test

The CAI tests were conducted on sandwich specimens after each impact and each healing cycle. Each test contained five effective specimens. For comparison purposes, five effective specimens without impact were also tested using the same anti-buckling fixture as controls. The test results are shown in Fig. 9. Two observations can be made: (1) each impact considerably decreases the CAI strength as compared to the control specimens. Also, the CAI strength gradually decreases as the impact cycle increases until the 6th impact cycle. For the 7th impact cycle, a significant rebound in CAI strength is observed; (2) each healing cycle recovers a considerable portion of the compressive strength lost due to impact. However, the healed specimens still have a slightly lower strength than the control specimen. This tendency holds true until the 6th healing cycle. For the 7th healing cycle, its strength after healing is higher than the control specimens. These observations can also be detailed by numerical analysis. For example, the CAI

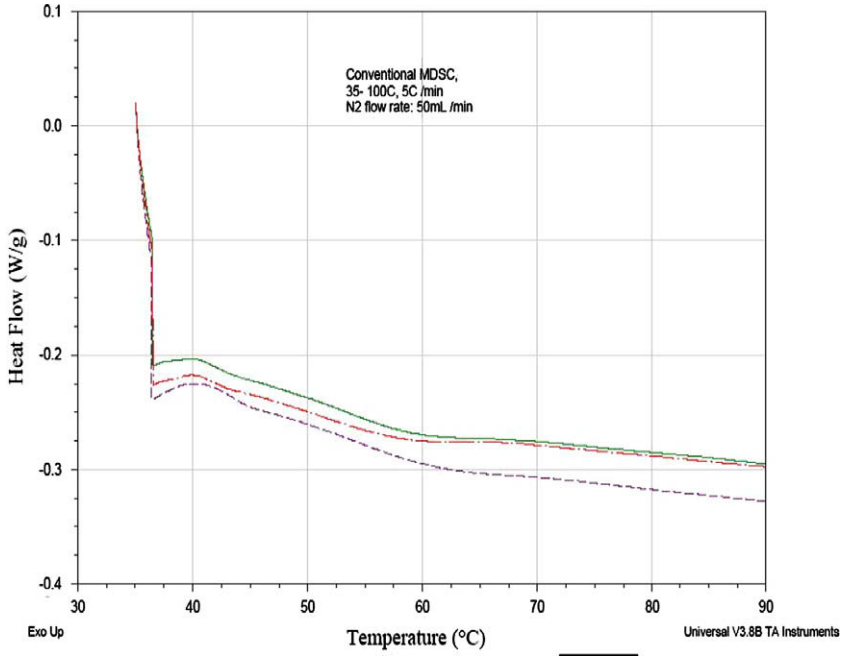

Fig. 4. Typical DSC result for the smart syntactic foam.

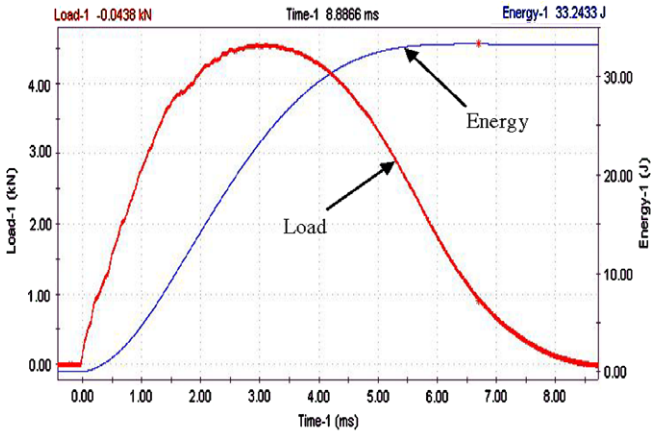

Fig. 5. Typical load–energy traces.

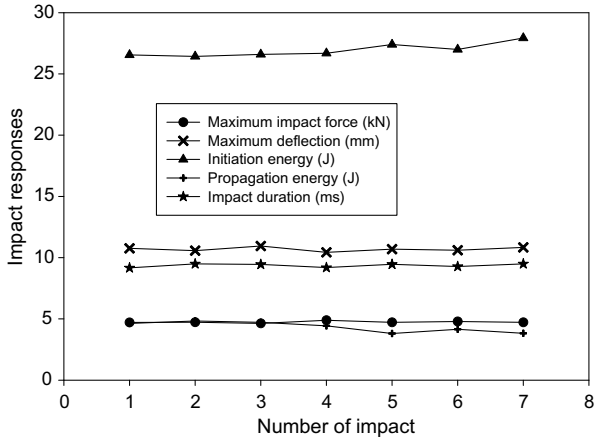

Fig. 6. Impact responses with impact cycles.

yield strength after the 1st impact is about 83.9% of the original yield strength without impact (control specimens, 12.23 MPa); after 1st healing, the yield strength is about 93.8% of the original strength. This suggests that the self-healing has recovered a major portion of the lost strength. After the 7th impact, the CAI yield strength is about 94.9% of the original yield strength; after the 7th healing, the residual strength is about 113.6% of the original yield strength. This suggests that after seven rounds of impact-healing cycles, the sandwich specimens are actually gaining some strength. This result echoes the impact test results, i.e., at the 7th impact-healing cycle, the sandwich panels are becoming better in resisting impact damage. It is believed that the healing process may have coupled with the post-curing of the foam.

In order to understand the post-curing effect, uniaxial compression test was conducted on a group of block foam specimens which experienced various additional post-curing time periods simulating the actual high temperature healing. The temperature was fixed at 100° C and the period of post-curing was equal to the time period of healing. One group of five specimens was post-cured for three additional hours to simulate the 1st healing cycle; another group of five specimens was post-cured for 21 additional hours to simulate the total healing hours up to the 7th healing. The specimen size was the same as the flat-wise specimens and the test was conducted per ASTM C365. The test results show that after the three additional hours of post-curing, the average yield strength of the foam is 5.10 MPa, which is about 0.81 MPa lower than the regularly cured specimens (5.91 MPa). This reduction may explain why the CAI strength of the sandwich specimens after 1st healing is only about 93.8% of the original strength. If the reduced strength of 0.81 MPa were added to the yield strength of the sandwich specimens after 1st healing (0.81 + 11.44 = 12.25 MPa), it is clear that the 1st healing would fully recover the original strength (12.23 MPa). From the C-scan images, it is clear that both impact and healing change the microstructure of the foam. The reduction in the yield strength of the foam after three additional hours of post-curing may be due to the changed microstructure which is unfavorable for the strength development. Of course, further study is needed to fully understand the mechanism.

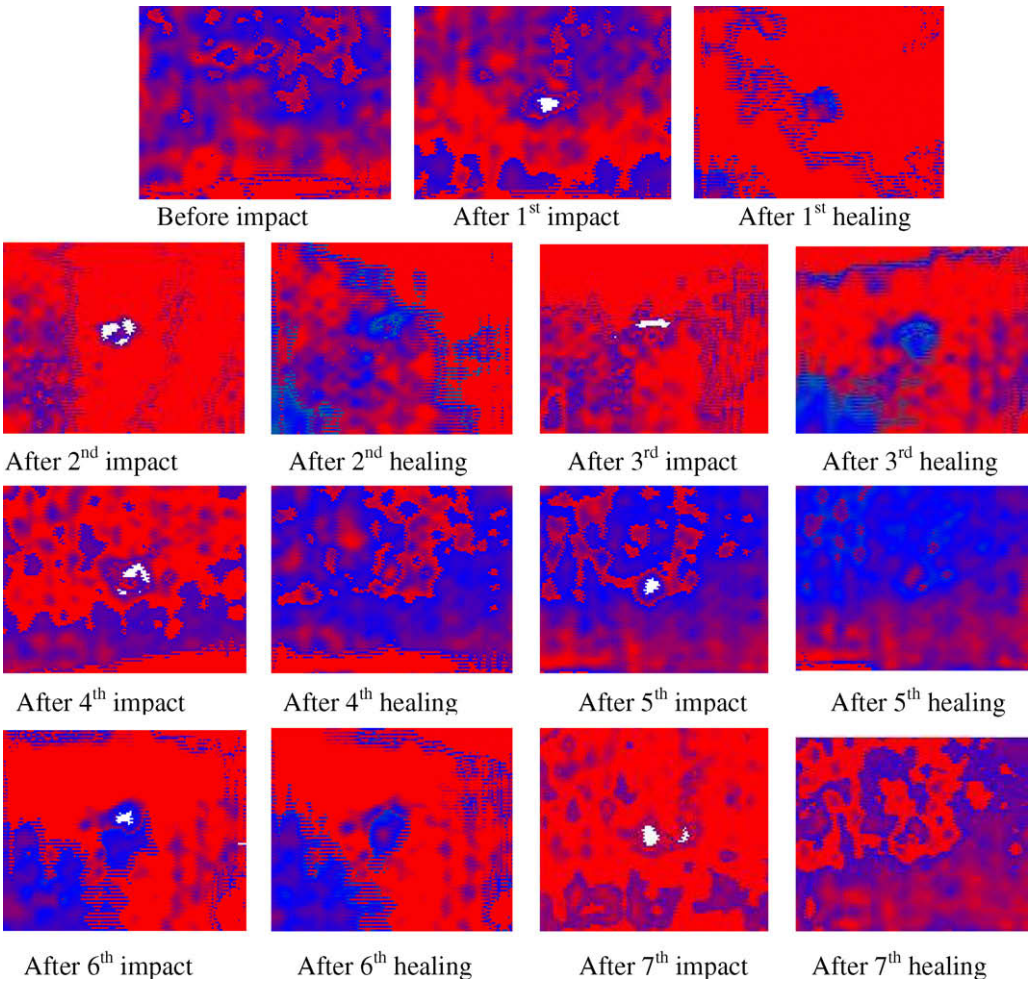

Fig. 7. C-scan images of the sandwich panels after each impact and healing cycle.

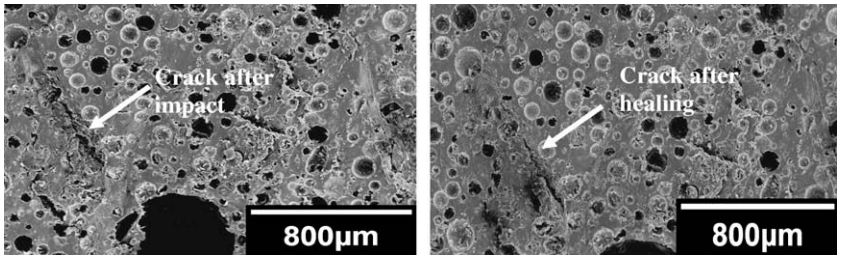

Fig. 8. SEM pictures showing the effect of healing on the microcrack.

After 21 h of additional post-curing, the yield strength of the foam becomes 7.60 MPa, which is about 7.60–5.91 = 1.69 MPa higher than the regularly cured foam without additional post-curing. This additional gain in strength is obviously due to the post-curing effect. If this additionally gained strength is removed from the sandwich panel after 7th healing (13.90–1.69 = 12.21 MPa), it is clear that this corrected yield strength is close to the original strength (12.23 MPa) (control sandwich panels).

It is noted that previous studies have shown that a certain correlations exist between impact damage and residual strength [30–33]. The key in establishing such a correlation is to quantify total impact damage area. Various techniques such as de-ply radiography technique [30], optical technique [31], and scanning acoustic methods [32,33] have been successfully used to quantify impact damage and correlate impact damage with residual strength. The correlation between the impact damage by C-scan and CAI strength in this study will be a topic of research in the future.

4. Conclusion

Based on the comprehensive test program, the following conclusions are obtained:

- The shape memory functionality of shape memory polymers can be used for the purpose of self-healing damage.
- The impact damage can be healed repeatedly.
- Compared with conventional polymer based syntactic foam, the SMP based foam has a considerable ductility.
- The glass transition temperature of the foam is similar to its polymer matrix with a much flattened peak.

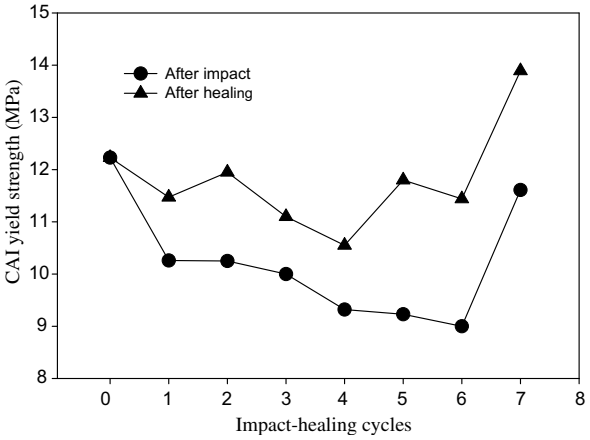

Fig. 9. Change of CAI yield strength with impact-healing cycles.

- The impact tolerance and load carrying capacity can be fully recovered after healing.
- There is a need to study the yield strength reduction with 3 h additional post-curing time.

Acknowledgements

This study is sponsored by the Louisiana Board of Regents/Economic Development Assistantship (EDA) and the NASA/EPSCoR under grant number NASA/LEQSF (2007-10)-Phase3-01. The authors would also like to acknowledge Dr. Xiogang Xie and Ms. Cindy Henk for their help in acquiring the SEM and TEM images and Dr. Kun Lian for help in obtaining the DSC results.

References

[1] Vance AP, Parks RM. Foam plastics in aircraft. J Cell Plast 1966;2:345–7.
[2] Hobaica EC, Cook SD. The characteristics of syntactic foams used for buoyancy. J Cell Plast 1968;4:143–8.
[3] Anderson TF, Walters HA, Glesner CW. Castable, sprayable, low density foams and composites for furniture, marble, marine. J Cell Plast 1970;6:171–8.
[4] Shutov FA. Syntactic polymer foams. In: Klempner D, Frisch KC, editors. Handbook of polymer foams and foam technology. Hanser publishers; 1991. p. 355–74.
[5] Shutov FA. Syntactic polymer foams. Adv Polym Sci 1986;73/74:63–123.
[6] Rizzi E, Papa E, Corigliano A. Mechanical behavior of a syntactic foam: experiments and modeling. Int J Solids Struct 2000;37:5773–94.
[7] Song B, Chen W, Frew DJ. Dynamic compressive response and failure behavior of an epoxy syntactic foam. J Compos Mater 2004;38:915–36.
[8] Bardella L, Genna F. On the elastic behavior of syntactic foams. Int J Solids Struct 2001;38:7235–60.
[9] Marur PR. Effective elastic moduli of syntactic foams. Mater Lett 2005;59:1954–7.
[10] Li G, Jones N. Development of rubberized syntactic foam. Compos A: Appl Sci Manuf 2007;38:1483–92.
[11] Li G, John M. A crumb rubber modified syntactic foam. Mater Sci Eng A 2008;474:390–9.
[12] Li G, Muthyala VD. Impact characterization of sandwich structures with an integrated orthogrid stiffened syntactic foam core. Compos Sci Technol 2008;68:2078–84.
[13] El-Hadek MA, Tippur HV. Dynamic fracture parameters and constraint effects in functionally graded syntactic epoxy foams. Int J Solids Struct 2003;40:1885–906.
[14] Gupta N. A functionally graded syntactic foam material for high energy absorption under compression. Mater Lett 2007;61:979–82.
[15] Nagy A, Ko WL, Lindholm US. Mechanical behavior of foamed materials under dynamic compression. J Cell Plast 1974;10:127–34.
[16] Lim TS, Lee CS, Lee DG. Failure modes of foam core sandwich beams under static and impact loads. J Compos Mater 2004;38:1639–62.
[17] Wouterson EM, Boey FYC, Hu X, Wong S-C. Fracture and impact toughness of syntactic foam. J Cell Plast 2004;40:145–54.
[18] Rittel D. Adiabatic shear failure of a syntactic polymeric foam. Mater Lett 2005;59:1845–8.
[19] Gould P. Self-help for ailing structures. Mater Today 2003;6:44–9.
[20] Balazs AC. Modeling self-healing materials. Mater Today 2007;10:18–23.
[21] White SR, Sottos NR, Geubelle PH, Moore JS, Kessler MR, Sriram SR, et al. Autonomic healing of polymer composites. Nature 2001;409:794–7.
[22] Alexeev A, Balazs AC. Patterned surfaces segregate compliant microcapsules. Presented at American Chemical Society 233rd National Meeting, Chicago; 2007.
[23] Hickenboth CR, Moore JS, White SR, Sottos NR, Baudry J, Wilson SR. Biasing reaction pathways with mechanical force. Nature 2007;446:423–7.
[24] Ratna D, Karger-Kocsis J. Recent advances in shape memory polymers and composites: a review. J Mater Sci 2008;43:254–69.
[25] Behl M, Lendlein A. Shape-memory polymers. Mater Today 2007;20:20–8.
[26] Liu Y, Gall K, Dunn ML, Greenberg AR, Diani J. Thermomechanics of shape memory polymers: uniaxial experiments and constitutive modeling. Int J Plast 2006;22:279–313.
[27] Koerner H, Price G, Pearce NA, Alexander M, Vaia RA. Remotely actuated polymer nanocomposites—stress-recovery of carbon-nanotube-filled thermoplastic elastomers. Nat Mater 2004;3:115–20.
[28] Cho JW, Kim JW, Jung YC, Goo NS. Electroactive shape-memory polyurethane composites incorporating carbon nanotubes. Macromolecular (rapid communications) 2005;26:412–6.
[29] Miaudet P, Derré A, Maugey M, Zakri C, Piccione PM, Inoubli R, et al. Shape and temperature memory of nanocomposites with broadened glass transition. Science 2007;318:1294–6.
[30] Kortschot MT, Zhang CJ. Characterization of composite mesostructures and damage by de-ply radiography. Compos Sci Technol 1995;53:175–84.
[31] Hirai Y, Hamada H, Kim JK. Impact response of woven glass-fabric composites––I: Effect of fibre surface treatment. Compos Sci Technol 1998;58:91–104.
[32] Todoroki A, Kobayashi H, Lee JG. Image analysis of delamination cracks in carbon-fibre composites by scanning acoustic microscopy. Compos Sci Technol 1994;52:551–9.
[33] Gao SL, Kim JK. Scanning acoustic microscopy as a tool for quantitative characterization of damage in CFRPs. Compos Sci Technol 1999;59:345–54.